3rd European supercritical CO2 Conference
September 19-20, 2019, Paris, France

2019-sCO2.eu-119

# DYNAMIC MODELING AND TRANSIENT ANALYSIS OF A MOLTEN SALT HEATED RECOMPRESSION SUPERCRITICAL $CO_2$ BRAYTON CYCLE

**Pan ZHOU***
EDF R&D China
Beijing, China
Email: Pan.zhou@edf.fr

**Jinyi ZHANG**
EDF R&D China
Beijing, China

**Yann LE MOULLEC**
EDF R&D China
Beijing, China

## ABSTRACT

Supercritical $CO_2$ power generation cycle is a promising power generation technology with a high potential to reach high thermal efficiency and high flexibility. In this work, a recompression cycle with intercooling and preheating is selected for the application of supercritical $CO_2$ cycle in concentrated solar power. Given the design boundary conditions, all the equipment are designed and optimized by in-house code, which gives a preliminary geometry for the equipment. The calculated geometries are then integrated into dynamic modules to simulate the off-design behaviors of equipment. Based on the developed equipment dynamic modules, a dynamic physical model of selected cycle is built in Modelica language implemented in Dymola. Part load transient scenarios are defined with technical constraints, such as minimum main compressor inlet temperature and minimum molten salt outlet temperature. With these key scenarios defined and constraints integrated into the model, sensitivity analyses are carried out to understand system dynamics. Global operation and control strategies for system protection, regulation and performance optimization are proposed and designed within MATLAB&SIMULINK to satisfy the pre-defined performance criteria. Finally, scenario simulations are done with the proposed control strategy and tuned control parameters to justify its feasibility.

## INTRODUCTION

Supercritical $CO_2$ ($sCO_2$) cycle has drawn much attention for power generation industry in recent years. Compared to water steam Rankine cycle, it has advantages of simpler cycle layout, more compact turbo-machineries and high potential to reach higher efficiency. In the meantime, $CO_2$ is inexpensive, dense and less corrosive than water at same high temperature, with an easily reachable critical point at 30.98℃ and 73.8 bar. $sCO_2$ power cycles could be applied to various potential heat source including nuclear power, coal-fired power, waste heat recovery and renewable energy sources such as concentrated solar power (CSP) and fuel cells [1].

CSP can provide carbon free and renewable energy to meet the energy demand. With integration of thermal storage system, CSP can decouple the solar-to-thermal and thermal-to-electric conversion regardless of the weather condition. However, the Levelized Cost of Electricity (LCOE) of CSP is still non-competitive (120$/MWh, average by 2020, reported in IRENA). Compared with the water steam Rankine cycle utilized in the existing CSP industry, $sCO_2$ cycles coupled with high temperature solar receivers and thermal storage are considered to be a solution to increase cycle efficiency and system flexibility, then to reduce the LCOE of CSP [2].

Dynamic modelling is a useful and efficient tool to help verify the equipment and to develop or optimize the control strategy of the power cycle. Yan [3] has carried out dynamic analysis and control system design for a nuclear gas turbine power plant, in which utilization of inventory control and by pass control is recommended respectively for keeping cycle efficiency and providing fast load regulation. Moisseytsev *et al.* [4] has developed a detailed dynamic model for a recompression $sCO_2$ Brayton cycle and has studied the cycle automatic control including inventory control, flow split control and etc. In the thesis of Carstens [5], a dynamic model for a $sCO_2$ recompression cycle of 600 MWth has been developed and part load simulation has been carried out with designed PID controllers.

In this work, pre-design of a 10 MWe recompression with intercooling and preheating $sCO_2$ Brayton cycle for CSP using molten salt as heat transfer fluid has been carried out and a dynamic model has been developed in Dymola with Modelica language. This cycle was designed for Shouhang – EDF demonstration project signed in 2018, with the objective of retrofit the Shouhang 10MWe CSP plant with $sCO_2$ Brayton cycle before the end of 2020. Transient analysis, temperature control and part load control have been carried out to analyze the dynamic behavior of the model and to study different control strategy for cycle part load.

* corresponding author(s)

DOI: 10.17185/duepublico/48879

## SYSTEM CONFIGURATION

The cycle studied in this work is a recompression cycle with intercooling and preheating, which is designed for a net power output of 10MWe and is optimized to work with molten salt between 530 ℃ and 290 ℃. The cycle layout is presented in Figure 1 with main part-load control systems. Auxiliary compressor (AC) is for recompression. The intercooling aims at minimizing the compressor work by cooling the $sCO_2$ fluid, which increases the density of $sCO_2$ [1]. On the other hand, the preheating helps increasing the utilization of molten salt while maintaining a high efficiency. The minimum cycle temperature and pressure are selected to be 35 ℃ and 82.1bar for the consideration of the sharp variations of sCO2 properties near its critical point. Detailed cycle parameters are presented in Table 1, which are optimized statically to achieve the highest output power.

**Table 1** Key parameters of 10 MWe sCO2 Brayton cycle

| Parameter | Unit | Value |
|---|---|---|
| Turbine inlet temperature | ℃ | 467.6 |
| Turbine inlet pressure | bar | 250 |
| Turbine mass flow rate | kg/s | 137.7 |
| MC inlet temperature | ℃ | 35 |
| MC inlet pressure | bar | 106.3 |
| Recompression split ratio | - | 27.74% |
| Molten salt inlet temperature | ℃ | 530 |
| Turbine power | MWe | 16.1 |
| Main compressor power | MWe | 2.4 |
| LTR heat exchanged | MW | 20.8 |
| HTR heat exchanged | MW | 26.5 |
| Net power output | MW | 10 |

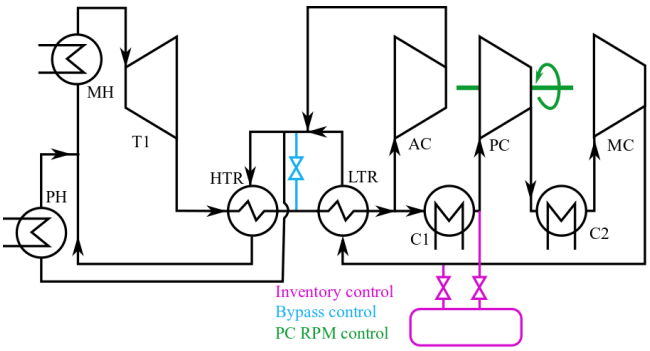


**Figure 1** System configuration of 10MWe Recompression intercooling and preheating sCO2 Brayton cycle

Molten salt/$CO_2$ heater, as the primary heater, is used to avoid the high challenge from high-pressure receiver design and to keep the advantage of full decoupling between sunshine and power generation. For the cooling, air cooler is used but with an indirect scheme: $CO_2$ is cooled by water that circulates in a closed loop while water is cooled by air cooler. Therefore, there will be no challenge on the resource of water on site. Figure 25 presents the yearly temperature in Dunhuang. In the hottest day, the maximum temperature is 38 ℃ which will be a challenge to the cooling system. However, it could be observed that the daily temperature difference is very high in Dunhuang, which is an ideal case for cold storage to guarantee the operation of cooler. $CO_2$ inventory system is also implemented as one of the main measures for load control, and it serves also as the main storage system during system startup and shutdown. The charge point is set before the inlet of the pre-compressor (PC, compressor located before the main compressor of the cycle) as the pressure at this point is the lowest in the cycle. In the same way, the discharge point is designed after the main compressor where the pressure is highest in the cycle. PC is designed to work at variable speeds, as another measure for load regulation.

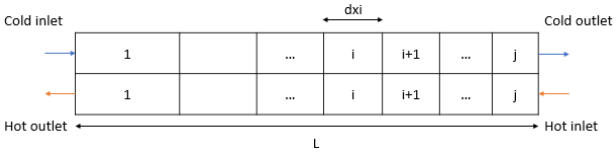


**Figure 2** Inhomogeneous discretization of PCHE

## PRE-DESIGN OF EQUIPMENT

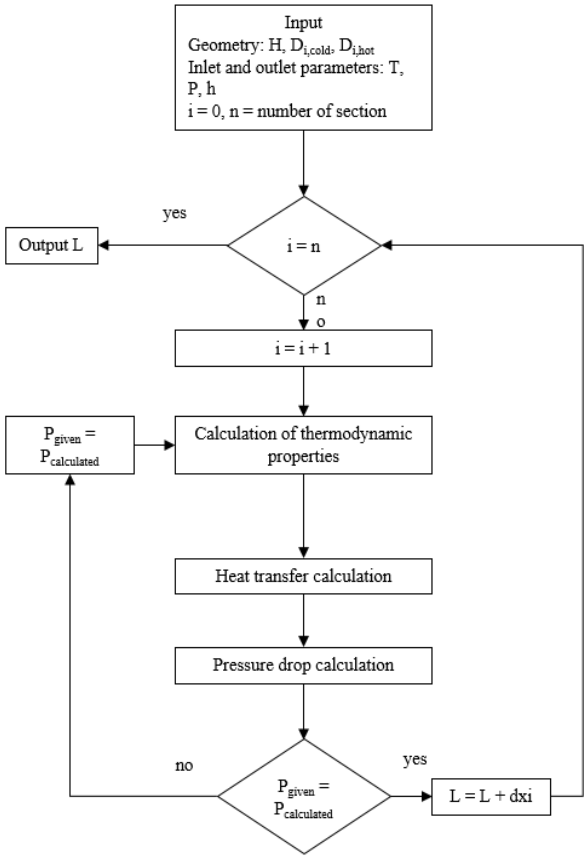


**Figure 3** Algorithm of heat exchanger pre-design tool

To establish the dynamic model, it is necessary to define the geometry of every component in the cycle. Therefore, pre-design is carried out for each component in excel.

### 1. Heat exchangers

Since they are used in most $sCO_2$ Brayton cycles, including those in SNL and Echogen [6], Printed circuit heat exchangers


DOI: 10.17185/duepublico/48879

(PCHE), with straight channel have been chosen in this work to represent the two recuperators of the cycle. The pre-design tool for PCHE utilizes inhomogeneous discretization method as showed in figure 2, which means that the heat exchanged for each section remains constant.

Study has been done to choose an appropriate number of sections (Ns) for pre-design. It was found that for Ns > 20, the design parameter given by the tool remains stable. As a result, 20 has been chosen for the number of section in the calculation of pre-design. The model considers a 1-D thermal conduction and the global heat transfer equation is presented below and the signification of parameter is listed in chapter nomenclature.

$$\frac{1}{K_i S_{min,i}} = \frac{1}{hc_{cold,i} \times S_{cold,i}} + \frac{1}{hc_{hot,i} \times S_{hot,i}} + \frac{e}{\lambda S_{min,i}}$$

$$S_{min,i} = Min\left(S_{hot,i}, S_{cold,i}\right)$$

Figure 3 represents the algorithm of geometry calculation for the pre-design tool. This algorithm calculates the length of PCHE by importing the height H of PCHE, hot and cold side channel diameter $D_{i,hot}$ and $D_{i,cold}$ and inlet and outlet thermodynamic properties temperature T, enthalpy h and pressure P. Calculation begins from the section one (counted from cold side). In each section, the thermodynamic properties are calculated by NIST REFPROP and then followed by heat transfer and pressure drop calculations. Gnielinski's correlation [7] is used to determine the heat transfer coefficient, listed in Table 3. The pressure of each section is supposed to be constant in the calculation and it was corrected after the calculation of pressure drop. The Darcy factor is determined by Haaland's correlation [8].

**Table 2** Geometry of heat exchanger determined by pre-design tool.

| | *LTR* | *HTR* | *C1* | *C2* | *PH* | *H1* |
|---|---|---|---|---|---|---|
| Length (m) | 0.93 | 0.88 | 27.2 | 12.5 | 11.8 | 11.8 |
| Height (m) | 1.53 | 2.16 | - | - | - | - |
| $D_{cold}$ (mm) | 0.82 | 0.85 | 750 | 640 | 522 | 761 |
| $D_{hot}$ (mm) | 1.50 | 1.41 | 0.03 | 0.03 | 0.03 | 0.03 |
| U (W/m$^2$/K) | 1679 | 1233 | 1047 | 1502 | 540 | 501 |

With this algorithm to calculate the length of heat exchanger, the pre-design tool minimizes the estimated price by varying the channel diameter of both sides and height of the PCHE. As for the optimization constraints, pressure drop for both sides was set to be 1 bar which is fixed for the cycle design and the minimum channel diameter is set to be 0.5 mm.

The heater and cooler utilized in the cycle are Shell and Tube heat exchangers (STHX). The pre-design process of STHX is similar with that of PCHE except for the calculation of pressure drop which is different for tube and shell sides. The calculation of pressure drop in both sides followed the correlations described in Kakaç's book [9]. Table 2 represents the result of heat exchanger pre-design. For STHX, cold side diameter represents shell internal diameter.

## 2. Turbomachinery

For turbo-machinery, predesign of centrifugal compressor and radial turbine of single stage has been carried out. In general, the preliminary design of turbomachinery consists of rotor calculation, stator calculation and performance estimation which includes different types of losses. In this work, a one-dimensional meanline design approach described by Ventura et al. [10]was applied for the pre-design of radial turbine. Oh et al [11] published an optimum set of empirical loss models for the performance estimation of centrifugal compressor. Expected isentropic efficiencies of compressor and turbine are 80% and 85% respectively.

With the help of these two approaches, geometry of turbomachinery was obtained, which was used for the off-design. Off-design generates curves of correlation between efficiency η and mass flow rate Q and also correlation between pressure ratio PR and mass flow rate Q for each rotation speed.

In dynamic model, it is preferred to introduce the performance curves to represent the dynamic behavior of turbomachinery for simplicity of dynamic model. However, the general performance curves are charts with 5 dimensions representing inlet temperature, inlet pressure, mass flow rate, rotation speed and efficiency or pressure ratio respectively, which still increases the complexity of the dynamic model. As a result, the 5-D performance curves were nondimensionalized into a 2-D chart according to the approach described in the thesis of M. Dyreby [12]. Those 2-D charts represent the relation between modified flow coefficient $\phi^*$ and modified efficient $\eta^*$ or modified head coefficient $\psi_i^*$, which are showed below:

$$\phi^* = \frac{Q}{\rho U D^2}\left(\frac{N}{N_{design}}\right)^x$$

$$\psi_i^* = \frac{\Delta h_i}{U^2}\left(\frac{N_{design}}{N}\right)^y$$

$$\eta^* = \eta\left(\frac{N_{design}}{N}\right)^z$$

The values of x, y and z are chosen according to the case studied and to the result of nondimensionalization. N represents the rotation speed. $N_{design}$ is the designed rotation speed. D is the impeller diameter and U is the impeller tip speed.

## DYNAMIC MODELING

The dynamic physical model of this cycle is developed with Modelica language implemented in Dymola. Modelica is an equational and object-oriented modeling language, whose compilers translate the equational models to imperative program such as C++ to generate executable code [13]. The simulation software platform Dymola is a simulation and modeling tool for large and complex system, composed of component models, in domains within automotive, aerospace, energy and other applications.

In this work, a complete system model has been developed in Dymola, which is composed of several component models such as turbomachinery, heat exchanger and other models. The


DOI: 10.17185/duepublico/48879

models were developed based on user-defined components and ThermoSysPro – a library of component models which is used for simulation and modeling of power plants, developed by El Hefni [13]. Each component is developed and then validated before being integrated into the full system.

The thermodynamic properties of $CO_2$ are calculated by REFPROP integrated in Dymola. As all the components in the system operate in supercritical phase, they are modeled as pure phase modules. For simplification, $sCO_2$ is separately cooled by water in Cooler 1 and 2 because the air cooler is not modelled in the system. In cycle pre-design, the pressure drop of valves was not considered but in dynamic model, the valve models brought certain pressure drop, which made a slight difference on the parameters between designed cycle and dynamic model. However, this difference should not have major impact on the dynamic behavior of the system.

### 1. Mass, Energy and Momentum Balance

The mass, energy and momentum conservation are fundamental laws that represent the thermal-hydraulic behavior of a fluid. Generally, a zero-dimension approach is used for thermal process modeling. As a result, the following three equations are used in the dynamic modeling:

$$V\cdot\left(\frac{\partial\rho}{\partial p}\frac{\partial p}{\partial t}+\frac{\partial\rho}{\partial h}\frac{\partial h}{\partial t}\right)=\sum Q_{in,i}-\sum Q_{out,i}$$

$$V\left(\left(h\frac{\partial\rho}{\partial p}-1\right)\frac{\partial p}{\partial t}+\left(h\frac{\partial\rho}{\partial h}+\rho\right)\frac{\partial h}{\partial t}\right)=\sum Q_{in,i}\cdot h_{in,i}-\sum Q_{out,i}\cdot h_{out,i}$$

$$L\frac{dQ}{dt}=A\cdot\left(p_{in}-p_{out}-\Delta p\right)$$

Q represents mass flow rate, h represents specific enthalpy and p represents pressure. Subscript in and out mean component inlet and outlet properties, all the properties without subscript means the medium volume average property in the component.

### 2. Heat exchanger models

Figure 4 represents the configuration of user-defined PCHE model in Dymola which consists of three parts: cold side tube, hot side tube and heat transfer wall. Applying the geometry given by pre-design, the tube model simulates pressure drop and heat transfer process which is considered to be the same in each parallel channel and a 1-D thermal conduction was considered in this model.

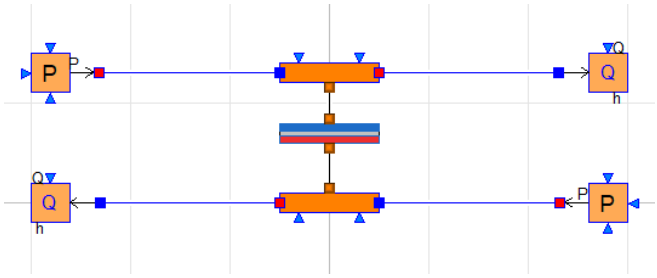


**Figure 4** Configuration of user-defined PCHE model in Dymola

Table 3 summarizes the correlations used in the calculation of heat transfer coefficient and pressure drop for PCHE and STHX. Unlike inhomogeneous discretization used in pre-design, homogeneous discretization is applied in the dynamic model in order to decrease the number of equations to be solved, as well as to decrease the simulation time of the model. The heat transfer wall represents a series of thermal resistances between cold fluid and hot fluid.

The study of the influence of the number of sections (Ns) on the precision of the dynamic model compared to predesign is carried out to find a trade-off between precision and complexity of the model. The relative difference between achieved duty of dynamic model and target duty represents the precision of the model. The model is firstly verified at steady-state by comparing the heat transfer and pressure drop results with the target values and then several scripts are carried out to check the dynamic behavior of the model.

**Table 3** Correlations for heat transfer coefficient and pressure drop calculation of PCHE and Shell & Tube heat exchanger.

| | Heat Transfer | Pressure drop |
|---|---|---|
| PCHE | Laminar [3]: $Nu = 4.089$<br>Transitional: linear interpolation between laminar and turbulent flow<br>Turbulent: Gnielinski [3] $Nu=\frac{\left(\frac{f_D}{8}\right)\times(Re-1000)\times Pr}{1+12.7\times\sqrt{\frac{f_D}{8}}\times\left(Pr^{\frac{2}{3}}-1\right)}=\frac{h_i\times d_i}{k_t}\ for\ Re>10^4$<br>$f_D=4\times(1.58\ln Re-3.28)^{-2}$ | Laminar [3]: $f=63.2/Re$<br>Transitional: linear interpolation between laminar and turbulent flow<br>Turbulent: Chen (1979) [3] $f=\left(3.48-1.7372\ln\left(2\epsilon-\frac{16.2426\ln A}{Re}\right)\right)^{-2}$<br>$A=\left(\frac{(2\epsilon)^{1.1098}}{6.0983}+\frac{7.149}{Re}\right)^{0.8981}$ |
| Shell & Tube | Same as turbulent regime of PCHE | |


DOI: 10.17185/duepublico/48879

### 3. Turbomachinery

For each dynamic model of turbomachinery, two 2-D charts obtained from pre-design were integrated:

$$\eta^* = f(\phi^*)$$
$$\psi_i^* = f(\phi^*)$$

The rotation speed of turbomachinery is given by user, which could be fixed or variable. Other parameters are calculated according to the two equations above and the inlet and outlet conditions of turbomachinery model.

## TEMPERATURE CONTROL LOOPS

In this work, four basic Proportional-Integral-Derivative (PID) controllers are integrated in the system to ensure that the turbomachinery is in the safe operation region and that the molten salt is beyond its freezing point.

PID controllers were designed in Matlab PID tuner. As design constraints, the phase margin and gain margin are set to be respectively higher than 60 deg and 60 dB. A maximum overshoot of 5% was allowed in order to satisfy the demand of rising time and oscillation was not accepted.

PID controllers of main compressor inlet temperature (MCIT) and Pre-compressor inlet temperature (PCIT) are integrated in the cooling system. They respectively control the inlet temperature of MC and PC to 35 ℃ by manipulating the mass flow rate of cooling water in C1 and C2 in case of sharp properties variation of $sCO_2$ near the critical point, which could influence the operation of the compressors. These two controllers are important for system part-load during which MCIT and PCIT variation commonly occurs. As mentioned before, the cooling system is designed to be an air cooler which cool down the water for the cooling of $sCO_2$ fluid. Although the air cooler was not integrated in the dynamic system, its effect on cooling water temperature cannot be ignored. If the air temperature decreases, e.g. due to the diurnal temperature difference, the cooling water temperature will drop, which leads to the variation of MCIT and PCIT and also to the system efficiency and power output.

Molten salt outlet temperature (MSOT) is controlled to 290 ℃ by acting on the molten salt mass flow rate to avoid the molten salt freezing and overheating of cold storage tank. To control Turbine inlet temperature (TIT), the manipulated variable should be the openness of the valve that connects MC outlet and turbine inlet. In order to simplify the dynamic model, mass flow rate of the fluid through the valve was selected to be the manipulated variable. TIT is controlled not to exceed its operation temperature, namely 467.6 ℃. These two controllers avoid overheat of TIT and prevent the freezing of molten salt, which could block the molten salt pipe. These two controllers are also important during system part-load. Moreover, the molten salt inlet temperature could be not stable because it is sensible to the solar irradiation and molten salt control which depends on real time weather and it also has influence on TIT.

## PART LOAD CONTROL STRATEGY

Part load control is significant in power plant as the output power should satisfy the demand of grid. Several control strategies have been proposed for the automatic control of gas turbine power plant which could be integrated in the $sCO_2$ Brayton cycle. Inventory control is an efficient control method for part load as the overall cycle efficiency is nearly constant during the control process [3]. Bypass control is preferable for rapid load control demand although it is less efficient than inventory control [3].

In this work, three control methods were separately integrated in the dynamic model and the study of their performance was carried out: inventory control, bypass control and variable PC rotation speed control. PID controllers have been designed in Matlab and then integrated in dynamic model.

### 1. Inventory control

Inventory control uses two tanks of $CO_2$, and is able to manipulate fluid injection and releasing in the system to achieve part load operation of system. First tank is directly connected to injection and release points, which is at around 100 bar and 35 ℃. The pressure of this tank is maintained by a compressor which connect these two tanks. The injection and release is achieved by manipulating the openness of corresponding valves. The released sCO2 will be cooled before enter the first tank. The charge and discharge of $CO_2$ in the cycle can be carried out at different points of the cycle. It is typically preferred to inject at low pressure points, e.g. inlet of PC and to release at high pressure points, e.g. outlet of MC. In this work, the charge point is selected to be at PC inlet with a $sCO_2$ tank of 160 bar and 35 ℃ and the cycle discharges at MC outlet to a tank at 83 bar. These two tanks are designed to maintain constant pressure during inventory charging and discharging. During discharge, the valve between MC downstream and discharge point is opened, the mass flow rate and pressure of the whole cycle decrease which leads to the drop of load.

Inventory control is to control the load of the system by manipulating the mass flow rate of the fluid through charge or discharge valve as showed in Figure 1. As the system temperature is changed during part load, the MCIT and PCIT should be controlled at 35 ℃ to avoid transcritical phenomena and instability of compressor operation. Moreover, TIT and MSOT controller should be integrated in the system. The rotation speed of turbomachinery is kept constant during inventory control. In addition, the inlet pressure of PC should be monitored in case of reaching critical pressure.

### 2. HTR & Heater & Turbine Bypass Control

By pass control achieves part load by venting fluid from LTR cold outlet to LTR hot inlet so that HTR, heaters and turbine are bypassed as showed in Figure 1. Turbine output power will therefore decrease which leads to the drop of load.

During the bypass control, the load is controlled by manipulating the mass flow rate through the bypass valve. Similarly to inventory control, elementary controllers of MCIT, PCIT, TIT and MSOT should be integrated.

### 3. Variable PC rotation speed control


DOI: 10.17185/duepublico/48879

In this work, PC is designed to be in a separated shaft in order to help performing the start-up, shut down and part load of the cycle. Once the rotation speed of PC decreases, the mass flow rate and pressure ratio of the turbomachinery will decrease, which leads to the drop of load. However, the achievable load variation of this method is limited. For this method, there is no charge or discharge point in the cycle. Therefore, the total mass of $CO_2$ in the cycle will keep constant and the mass flow rate of $CO_2$ in the cycle will not have big variation. The distribution of pressure in the cycle will keep stable. As a result, the load will not much vary. On the other hand, this method could be combined with inventory control which has injection and releasing point in the cycle.

## RESULTS AND DISCUSSION

### 1. Inventory control

In this work, scenario of discharge to 70% load with inventory control has been carried out for the system without and with elementary PID controllers so that the effect of elementary controllers (basic loop control) can be discussed.

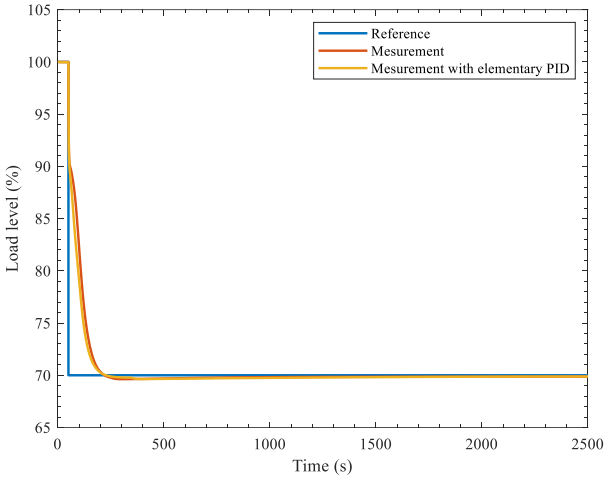


**Figure 5** Load level during discharge

**Without elementary controllers**, the controller for inventory control reacts immediately when a step reference signal is sent as showed in Figure 5. The load of system decreases and reaches the reference value after an overshoot of 0.9%. Figure 6 represents the variation of cycle net efficiency during the discharge. It can be observed that the efficiency decreases from 35.67% to 31.74% and then rises to 33.39%: a drop of 2.3% for efficiency which is higher than the same case for an ultra-supercritical Rankine cycle. At the beginning, reduction of efficiency is mainly caused by the initial decrease of TIT and the turbine inlet pressure as showed in Figures 7 and 8. Moreover, it can be observed in Figure 9 that the LTR hot side pinch increases 5 ℃, which is another cause for the decrease of efficiency. From figure 26 it can be observed that compared to 100% load, heat transfer efficiency decreased at 70% load so that LTR pinch increases. Then, TIT increases because the mass flow rate of molten salt is kept constant but the mass flow rate of $sCO_2$ in cycle decreases, which yields a slow increase of efficiency.

It should be noted that the cycle minimum pressure decreased to 70.5 bar which is below the critical pressure. Action needs to be taken to avoid this situation. A constraint could be added in the controller: when the PC outlet pressure is lower than a predefined safe pressure (e.g. 74bar), no intervention is applied to inventory control.

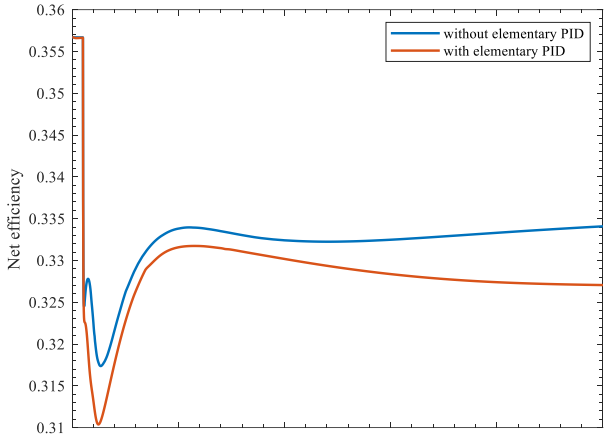


**Figure 6** Cycle net efficiency during discharge

As for the cooling system, it can be observed in Figure 11 that without elementary PID controller, PCIT decreases from 35 ℃ to 29 ℃ because the mass flow rate of cooling water is kept constant. However, MCIT decreases at the beginning, rises then to 37 ℃ and finally decreases slowly to 36 ℃ as showed in Figure 12. The drop at the beginning should be caused by the decrease of PC inlet temperature and $sCO_2$ mass flow rate. However, when the mass flow rate of $sCO_2$ decreases, according to the performance map of the compressor, the efficiency of PC decreases so that PC outlet temperature increases which leads to the increase of MCIT. From the discussion above, it can be concluded that it is important to add elementary PID controllers for TIT, MSOT, PCIT and MCIT.

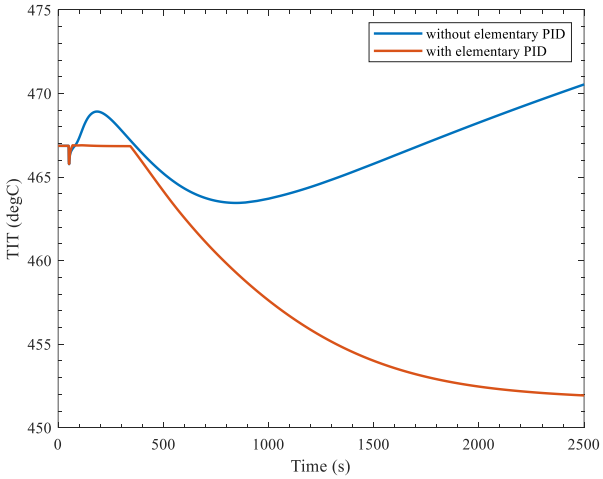


**Figure 7** TIT during discharge


DOI: 10.17185/duepublico/48879

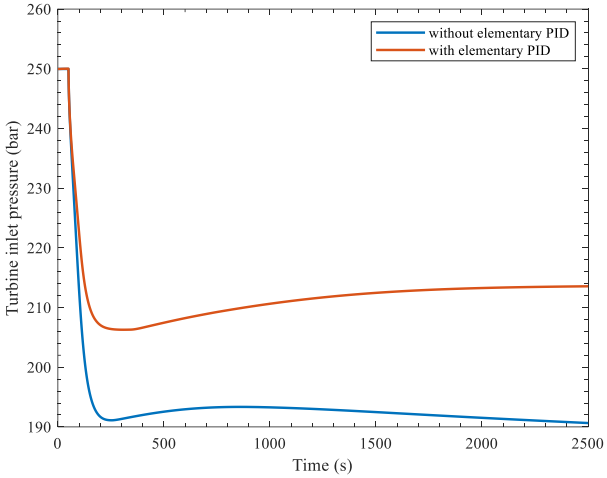


**Figure 8** Turbine inlet pressure during discharge

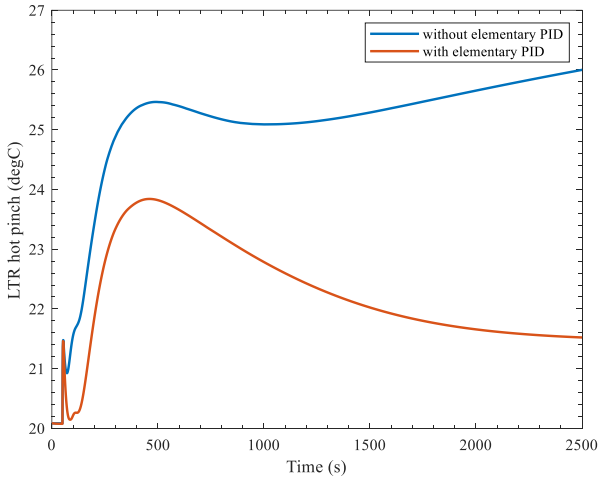


**Figure 9** LTR hot side pinch during discharge

**With elementary controllers**, it can be observed in Figures 7, 10 and 11 that TIT, MSOT and PCIT are controlled in their reference region. However, MCIT increases to 38.5 ℃, instead of 35 ℃, as showed in Figure 12. As stated in the last section, MCIT is controlled by manipulating the mass flow rate of C2 cooling water. It should be noted that there is a limit for augmentation of mass flow rate of cooling water because when it becomes too big, the water pressure drop will increase. In this scenario, the pressure drop already reached its highest value and the maximum allowed mass flow rate cannot satisfy the cooling of MCIT. As a result, the control of MCIT could not be achieved only by manipulating the mass flow rate of cooling water. In reality, the water is cooled by an aircooler. It is possible to act on the velocity of air in aircooler to manipulate the temperature of cooling water. And it can be observed in Figures 7 and 10 that with current TIT and MSOT controllers, TIT decreases while MSOT is kept constant at 290 ℃ because MS mass flow rate is reduced to help keep MSOT at 290 ℃ and there is no solution to increase TIT.

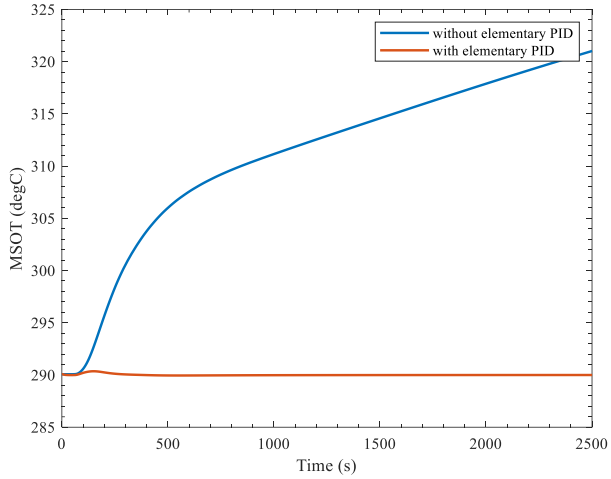


**Figure 10** MSOT during discharge

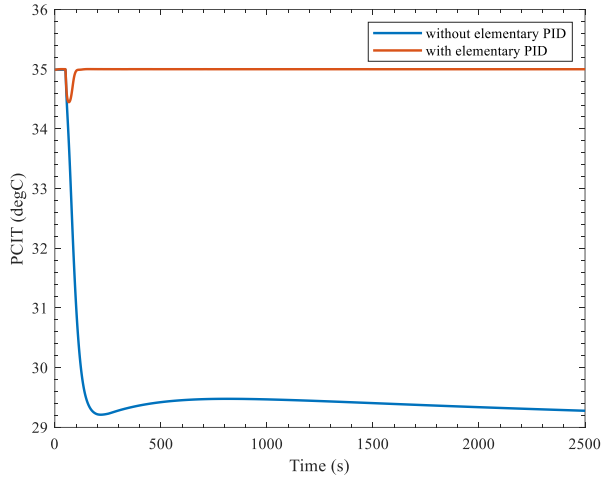


**Figure 11** PCIT during discharge

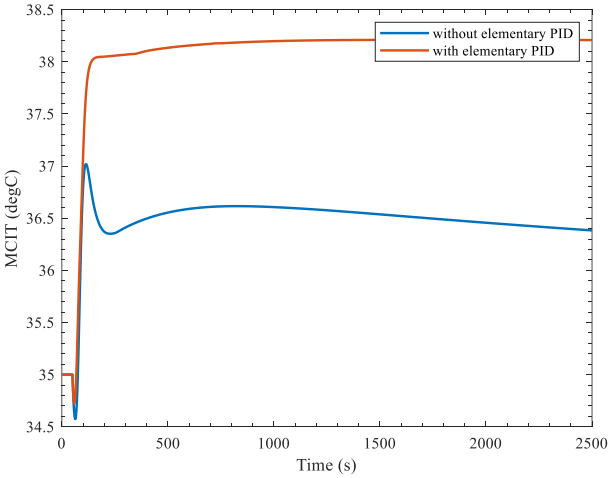


**Figure 12** MCIT during discharge


DOI: 10.17185/duepublico/48879

As showed in Figure 6, the cycle net efficiency decreased to lower value with elementary PID controller. It is mainly caused by the decrease of TIT since the mass flow rate of MS decreased to keep MSOT at 290 ℃. When the load decreased to 70%, the difference of cycle efficiency between scenario without and with elementary PID is 0.22%.

### 2. Bypass control

In this work, a scenario of discharge to 70% load with bypass control is carried out for the system and the effect of elementary controllers (basic loop control) is discussed.

**Without elementary controllers**, the bypass controller reacts extremely fast when a step signal of part load is sent as showed in Figure 13. However, it can be observed in Figure 14 that the cycle net efficiency drops from 35.66% to 26.34% because of the decrease in turbine inlet flow, which causes a decrease in output power. This leads to the continuous rise of TIT as showed in Figure 18. Bypass control has no significant influence on MCIT and PCIT which increases to 36 ℃ as showed in Figures 19 and 20.

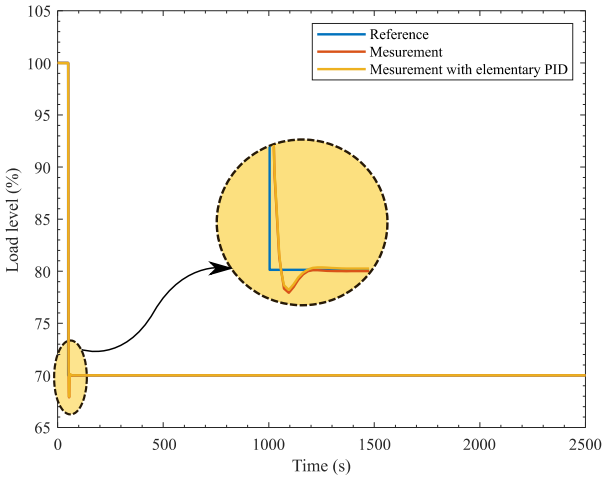


**Figure 13** Load level during bypass control

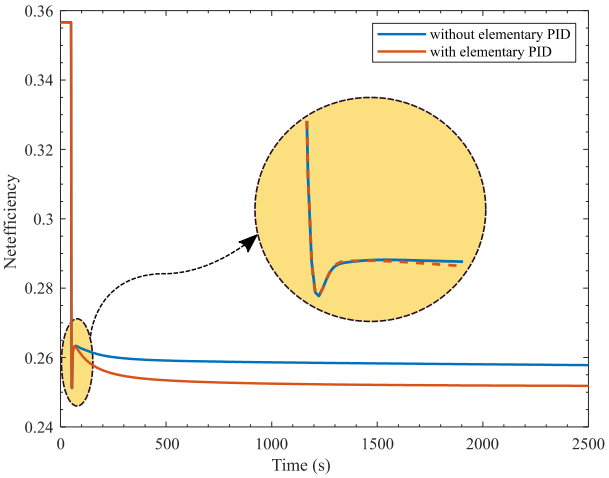


**Figure 14** Efficiency during bypass control

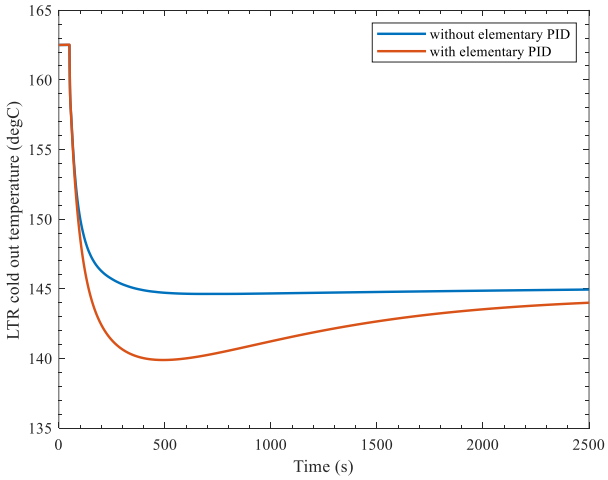


**Figure 15** LTR cold outlet temperature during bypass control

**After adding elementary controllers**, TIT, MSOT PCIT and MCIT have been well controlled.

However, bypass control brings challenge to PCHE. As showed in Figure 15, for a step response of part load, LTR cold outlet temperature drops from 162 ℃ to 150 ℃ in 40s in the beginning, which produces a large thermal stress of PCHE. Constraint needs to be added to the by-pass controller to avoid large thermal stress of PCHE. Reasonable ramp signal of load could be taken to slow down the drop of PCHE temperatures.

### 3. Variable PC rotation speed

Same part load scenario as the control strategy before has been carried out for the variable PC rotation speed control. However, limit on the variation of PC rotation speed restricted the level of part load. In this study, the design rotation speed of PC is 9500 RPM. Besides, the dynamic model could achieve a step of PC rotation speed from 9500 to 5000 RPM. As a result, scenarios of load decreasing from 100% to 90% without elementary control have been carried out for variable PC rotation speed control.

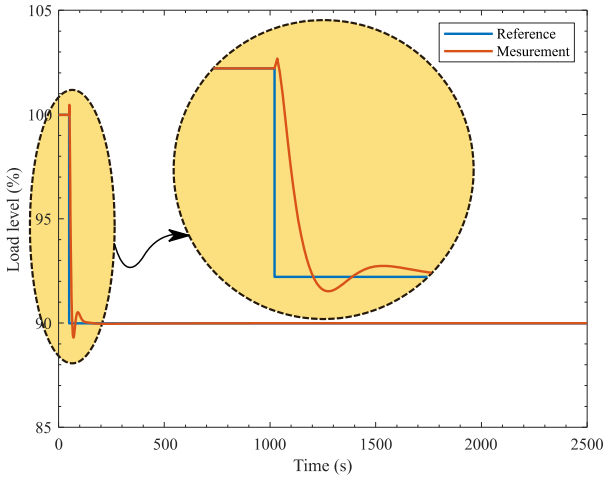


**Figure 16** Load level during part load without elementary PID


DOI: 10.17185/duepublico/48879

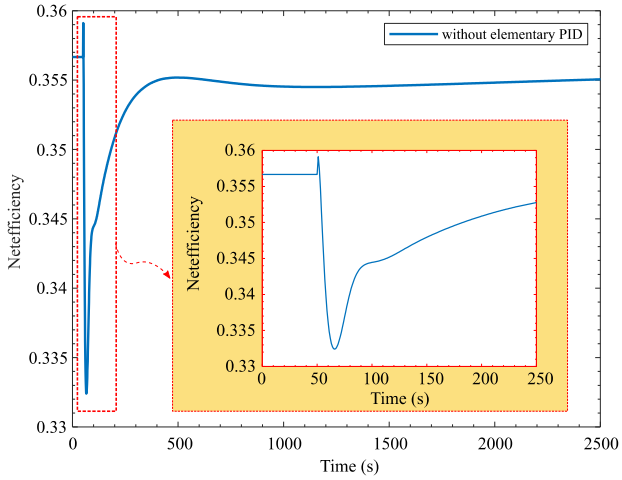


**Figure 17** Cycle Efficiency during part load without elementary PID

As showed in Figure 16, the load level decreases with the step reference and reaches 90% in a short time after an overshoot caused by the PID controller. The cycle efficiency decreases of 0.004% for load from 100% to 90%, which is smaller than 0.8% for inventory control and 3.22% for bypass control at same load level decrease. As showed in Figures 21 and 22, TIT and MSOT had the same variations as during inventory control. For the cooling part, both MCIT and PCIT decrease, especially MCIT that reaches the $CO_2$ critical temperature as showed in Figures 23 and 24. Therefore, elementary controllers need to be integrated for this control strategy.

### 4. Discussion

Three control methods for part load have been tested in this work. Inventory control could maintain the cycle efficiency within a certain range during part load but it is risky to realize a huge discharge flow because the minimum pressure of the cycle could go below the critical pressure. Moreover, the controllers for MCIT and PCIT are important for the proper operation of the compressors. Bypass control has the advantage of fast load but the cycle efficiency would have a significant drop and the gradient of temperature of PCHE should be monitored in case of high thermal stress. Variable PC rotation speed control can better keep the cycle efficiency than inventory control but it has its limit on the achievable load level and elementary controllers need to be integrated. It should be noted that the variable PC rotation speed control could be replaced by an inlet guide valve (IGV) at industrial scale.

It is possible to combine these three control methods to find an appropriate control strategy according to part load demand. For example, for part load from 100% to 50%, inventory control and bypass control could be combined to find a trade-off between load decreasing speed and cycle net efficiency [14]. Besides, bypass control and variable PC rotation speed control could be combined to achieve small load decline range.

## CONCLUSION

In this work, a dynamic model has been developed for a 10MWe $sCO_2$ Brayton cycle with detailed equipment pre-design and off-design. Fundamental physical laws and models found in open literature are utilized to develop main sub-models such as heat exchangers and turbomachinery. Although simplification has been done to reduce the complexity of the dynamic model, it remains a highly non-linear system of equations, with nearly 5000 equations. In particular, the sharp variations of $sCO_2$ properties near its critical point significantly slows down the resolution of this dynamic system.

Based on the dynamic model, three methods for achieving part load of system have been discussed, each with its own benefits and shortcomings. Inventory control could keep cycle efficiency but strict elementary controllers need to be integrated to guarantee the safe operation of turbomachinery and molten salt. Bypass control could achieve fast load, but will lose cycle efficiency. Variable PC rotation speed control could better maintain the cycle efficiency but is limited by its operation range. It can thus be concluded that elementary control of cooling and heating system is extremely important, as it impacts the actual performance of the cycle in operation. In this work, it is found that MCIT and PCIT could not be perfectly controlled by manipulating only the mass flow rate of cooling water because of huge water pressure drop engaged by the increasing mass flow rate. Additional measure should be taken to guarantee the safe operation of compressors. For example, the design of cooler could be modified for larger pressure drop. Moreover, the aircooler model could be integrated in the system so that besides water mass flow rate, the air velocity could be another manipulated variable. As for the heating system, a solution for increasing TIT should be found to avoid the possible reduction of TIT during inventory control. Although TIT and MSOT controllers are designed separately, they have influence on each other's behavior. As a result, it is necessary to design a better control strategy for these two parameters.

Finally, with these three part load methods, possible combination could be made for different part load scenarios according to their advantages. Normally, by-pass control could be selected for a fast and short-term part-load demand. However, if a long-term part-load is requested, by-pass control and inventory control could be combined: by-pass control is responsible for fast load regulation at the beginning and when the load reaches the desired value, the by-pass control could be replaced by inventory control to recover the cycle efficiency. In addition, variable PC rotation speed control and inventory control could be combined for faster and efficient part load control as discussed in previous paragraph. These possible combinations will be studied in the future work.

## NOMENCLATURE

| ***Symbols*** | |
|---|---|
| p | Pressure (MPa) |
| Q | Mass flow rate (kg/s) |
| T | Temperature (℃) |
| hc | Heat transfer coefficient ($W/m^2/K$) |
| S | Heat exchange Surface ($m^2$) |


DOI: 10.17185/duepublico/48879

| | |
|---|---|
| K | Global heat transfert coefficient ($W/m^2/K$) |
| $f_D$ | Darcy factor |
| f | Fanning factor |
| e | Thickness of heat exchanger wall |

***Greek symbols***

| | |
|---|---|
| $\eta$ | Efficiency |
| $\phi$ | Flow coefficient |
| $\psi$ | Head coefficient |
| $\lambda$ | Conductivity |

***Abbreviations***

| | |
|---|---|
| AC | Auxiliary compressor |
| C1 | Cooler 1 |
| C2 | Cooler 2 |
| $CO_2$ | Carbon dioxide |
| CSP | Concentrated solar power |
| HTR | High temperature recuperator |
| IC | Intercooling |
| LTR | Low-temperature recuperator |
| MC | Main compressor |
| MH | Main heater |
| MS | Molten salt |
| PC | Pre-compression / pre-compressor |
| PCHE | Printed circuit heat exchanger |
| PH | Preheating / preheater |
| RC | Recompression |
| $SCO_2$ | Supercritical $CO_2$ |
| STHX | Shell and tube heat exchanger |
| TIT | Turbine inlet temperature |

***Subscripts/superscripts***

| | |
|---|---|
| cold | cold side flow of heat exchanger |
| hot | hot side flow of heat exchanger |
| in | inlet flow |
| out | outlet flow |
| * | modified |

## REFERENCES


[1] Y. Ahn, S. Jun Bae, M. Kim, S. Kuk Cho, S. Baik, J. Ik Lee and J. Eun Cha, "Review of Supercritical CO2 power cycle technology and current status of research and development," *Nuclear Engineering and Technology,* pp. 1-15, 2015.

[2] M. Binotti, M. Astolfi, S. Campanari, G. Manzolini and S. Paolo, "Preliminary assessment of sCO2 power cycles for application to CSP solar tower plants," *Energy Procedia,* vol. 105, pp. 1116-1122, 2017.

[3] X. Yan, "Dynamic Analysis ans Control System Design for an Advanced Nuclear Gas Turbine Power Plat," Massachusetts Insititute of Technology, 1990.

[4] A. Moisseytsev, K. Kulesza and J. Sienicki, "Control System Options and Strategies for Supercritical CO2 cycles," Argonne National Laboratory, 2006.

[5] N. A. Carstens, "Control Strategies for Supercritical Carbon Dioxide Power Conversion Systems," Massachusetts Institute of Technology, 2007.

[6] M. Carlson, A. Kruizenga, C. Schalansky and D. Fleming, "Sandia Progress On Advanced Heat Exchangers For Sco2 Brayton Cycles," in *The 4th International Symposium - Supercritical CO2 Power Cycles*, Pittsburgh, 2014.

[7] J. Hesselgreaves, Compact Heat Exchangers, Pergamon, 2001.

[8] H. L. I. John and H. L. V. John, A Heat Transfer Textbook, Phlogiston Press., 2018.

[9] S. Kaka ç H. Liu and A. Pramuanjaroenkij, HEAT EXCHANGERS, CRC Press, 2012.

[10] A. V. Carlos, A. J. Peter, S. R. Andrew, P.-R. Paul and S. Emilie, "Preliminary design and performance esstimation of radial inflow turbines: an automated approch," *Journal of Fluids Engineering,* vol. 134, pp. 031102 1-13, 2012.

[11] H. Oh, E. Yoon and M. Chung, "An optimum set of loss models for performance prediction of centrifugal compressors," *Proceeding of the Institution of Mechanical and Engineer,* vol. 211, 1997.

[12] J. D. John, "Modeling the Supercritical Carbon Dioxide Brayton Cycle with Recompression," 2014.

[13] E. H. Baligh and B. Daniel, Modeling and Simulation of Thermal Power Plants with ThermoSysPro, Springer, 2018.

[14] J. Zhang, Z. Yang and Y. Le Moullec, "Dynamic modelling and transient analysis of a molten salt heated recompression supercritical CO2 Brayton cycle," in *The 6th International Supercritical CO2 Power Cycles Symposium* , Pittsburgh, 2018.



DOI: 10.17185/duepublico/48879

## ANNEX A: FIGURES FOR DIFFERENT CONTROL STRATEGY

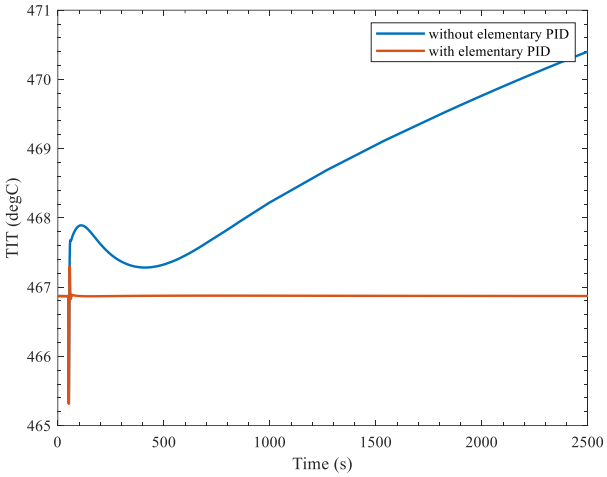


**Figure 18** TIT during bypass control

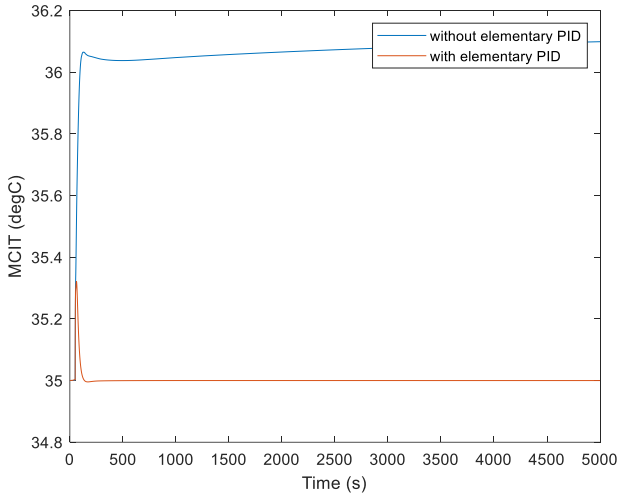


**Figure 19** MCIT during bypass control

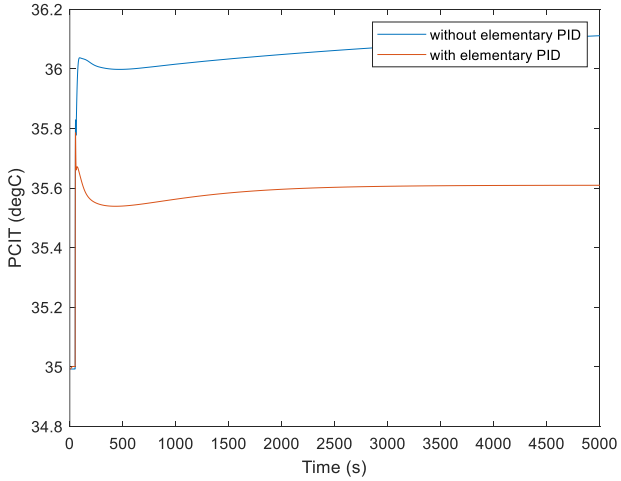


**Figure 20** PCIT during bypass control

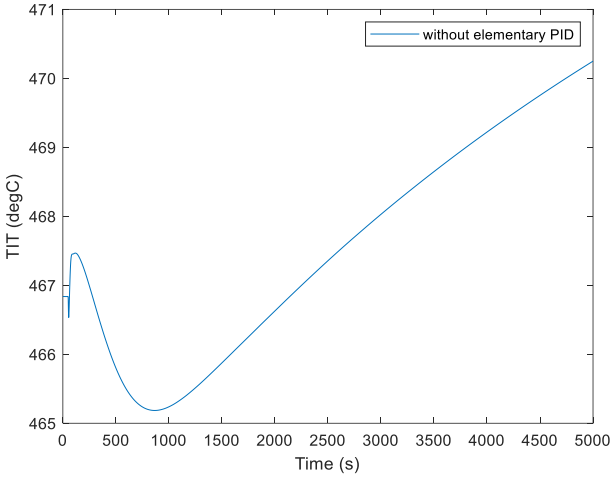


**Figure 21** TIT during part load by variable PC rotation speed

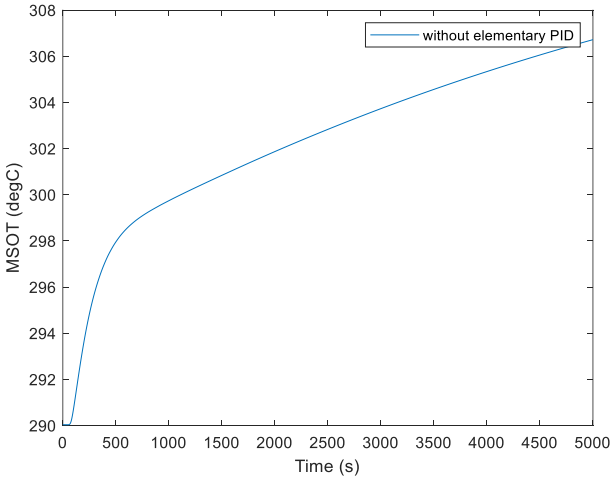


**Figure 22** MSOT during part load by variable PC rotation speed

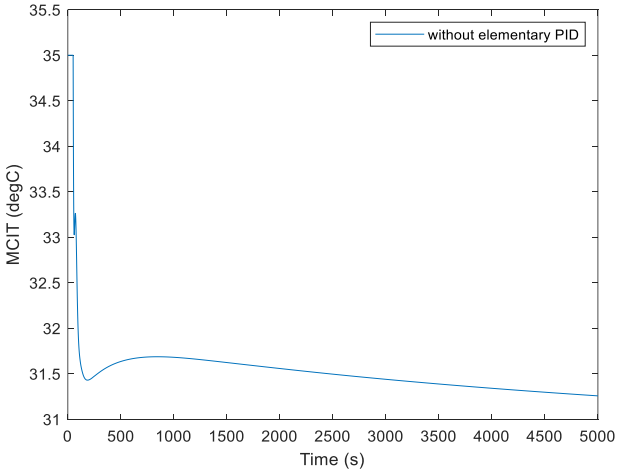


**Figure 23** MCIT during part load by variable PC rotation speed


DOI: 10.17185/duepublico/48879

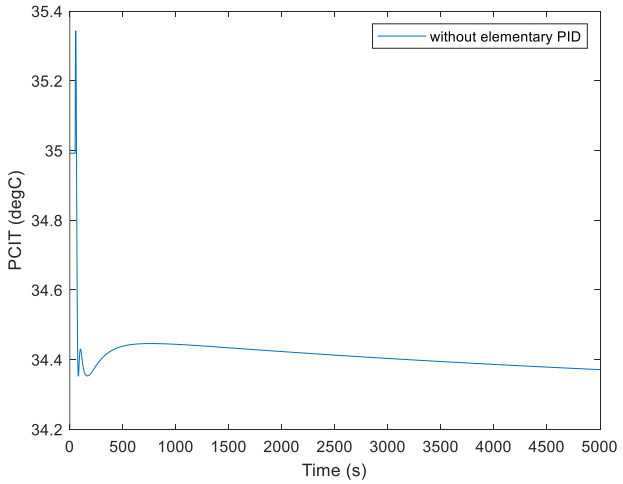


**Figure 24** PCIT during part load by variable PC rotation speed

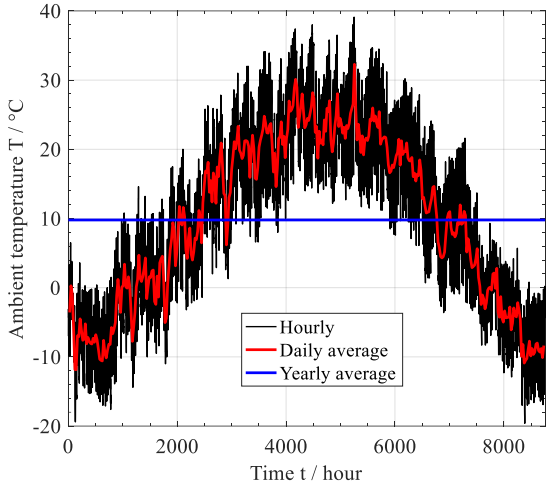


**Figure 25** Yearly temperature distribution in Dunhuang

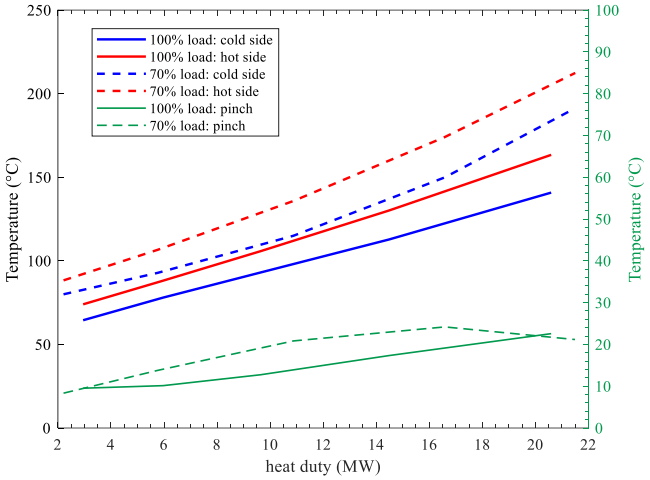


**Figure 26** Temperature - Heat duty diagram (left axes) and LTR pinch (right axes)


DOI: 10.17185/duepublico/48879

**DOI:** 10.17185/duepublico/48879
**URN:** urn:nbn:de:hbz:464-20191002-163136-9